Supplementary Information

Highly selective and sensitive detection of methyl mercaptan by heterostructural CdS/$(Sr_{0.6}Bi_{0.305})_2Bi_2O_7$ chemiresistor

Junqing Chang[a,c], Chaohao Hu[d], Zanhong Deng[a,c], Meng Li[a,b], Chengyin Shen[e], Shimao Wang[a,c], Longqing Mi[a,b], Ruofang Zhang[a,b], Qingli Zhang[a,c], Gang Meng[a,c,*]

[a] Anhui Provincial Key Laboratory of Photonic Devices and Materials, Anhui Institute of Optics and Fine Mechanics, and Key Lab of Photovoltaic and Energy Conservation Materials, Hefei Institutes of Physical Science, HFIPS, Chinese Academy of Sciences, Hefei 230031, China

[b] University of Science and Technology of China, Hefei 230026, China

[c] Advanced Laser Technology Laboratory of Anhui Province, Hefei 230037, China

[d] Guangxi Key Laboratory of Information Materials, School of Materials Science and Engineering, Guilin University of Electronic Technology, Guilin 541004, China

[e] Anhui Province Key Laboratory of Medical Physics and Technology, Center of Medical Physics and Technology, HFIPS, Chinese Academy of Sciences, Hefei 230031, China

[*]Corresponding author.

E-mail addresses: menggang@aiofm.ac.cn (G. Meng).

Keywords: Heterostructural CdS/SBO; Methyl mercaptan chemiresistor; Highly selective; Sulfurization-desulfurization

Fig. S1. Synthesis process of CdS/SBO nanomaterials.

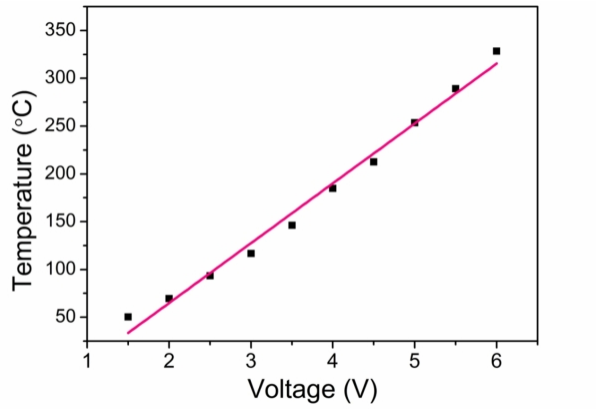

Fig. S2. The relationship between voltage and working temperature.

In order to test the thermal stability of CdS, the synthesized CdS powder samples were annealed in quartz crucibles at different temperatures (300 – 500 °C) and kept for 24 h (heating rate is 1 °C /min). The XRD (Fig. S3b) pattern shows that the diffraction peak pattern of the prepared CdS is consistent with the standard PDF card (JCPDS No. 89-0440). When the annealing temperature reaches 400 °C, the XRD pattern shows that

the phase of CdS has appeared some impurities. When the annealing temperature reaches 500 °C, the sample has undergone a complete phase transition, suggesting that the CdS material cannot work at higher temperature.

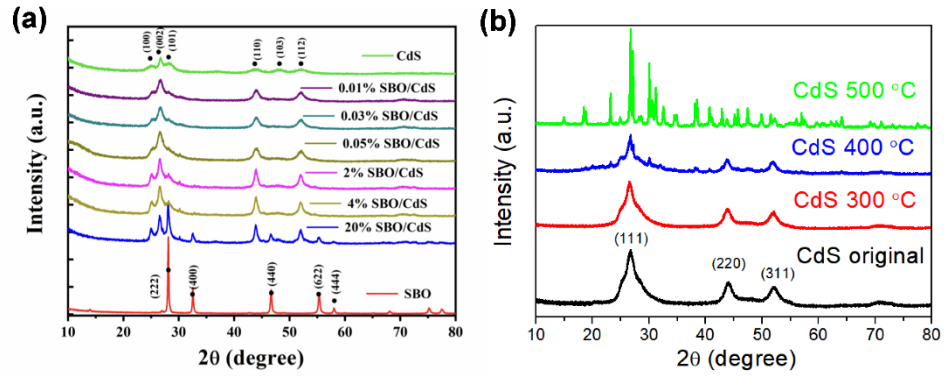

Fig. S3. (a) XRD patterns of SBO, CdS and CdS/SBO nanomaterials with different ratio. (b) XRD patterns of CdS at different annealing temperature (300 – 500 °C).

The FTIR spectra of the SBO, CdS and CdS/SBO nanomaterials are illustrated in Fig. S4f, which are similar to each other. The broad band at 3442 cm^{-1} and 1442 cm^{-1} are ascribed to the stretching vibration and in-plane deformation vibration of O−H groups[1], respectively, and the peaks centered at 2919 and 2852^{-1} can be attributed to C−H stretching vibration[2]. The asymmetric stretching vibrations of C=O and C–O–C appear at 1633 cm^{-1} and 1118 cm^{-1}, respectively[3, 4]. In addition, several strong peaks near at 618 cm^{-1} are caused by metal-oxygen bond vibrations in the as-synthesised nanomaterials[5, 6]. As shown in Fig. S4g, the SBO and CdS are direct semiconductors and show a visible absorption hence the band gap of SBO and CdS can be calculated as 1.25 eV and 2.32 eV, respectively (Fig. S4h).

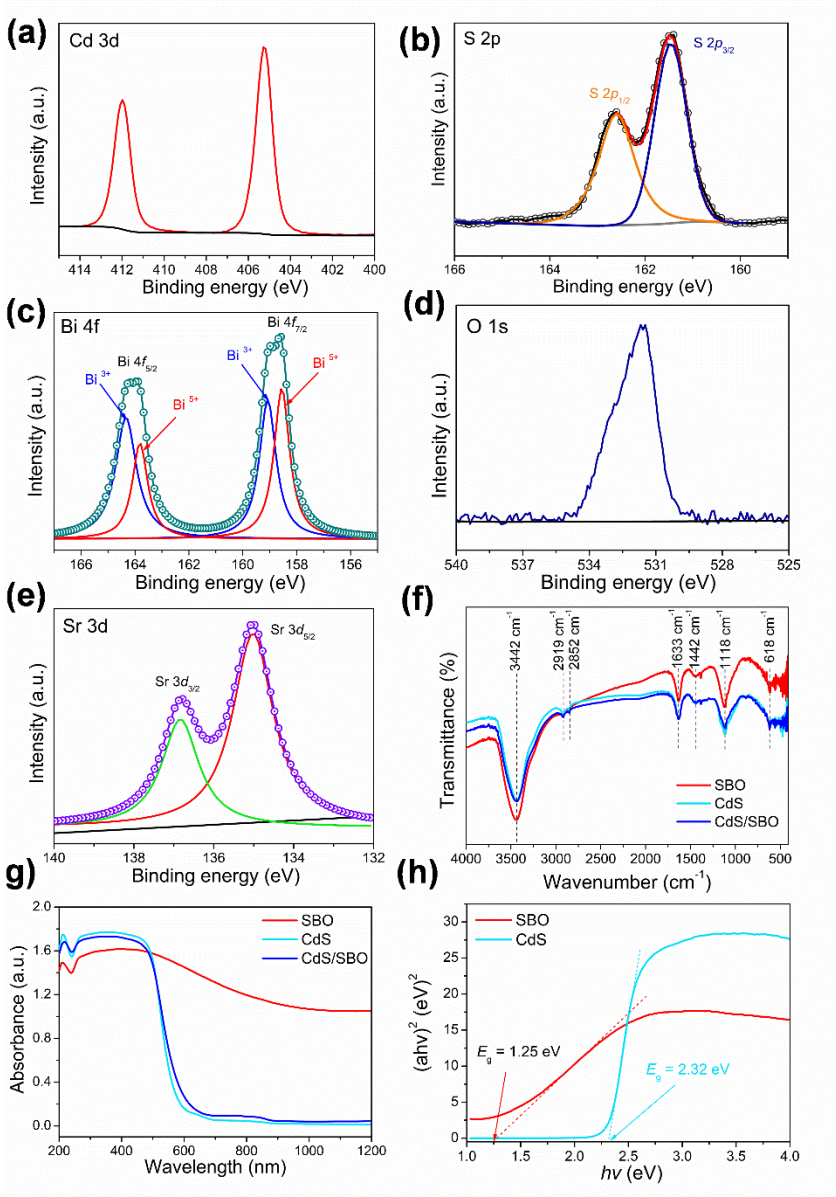

Fig. S4. (a) Cd 3d, (b) S 2p, (c)Bi 4f, (d) O 1s, (e) Sr 3d XPS spectra of CdS/SBO composite. (f) FT-IR spectra (g) UV-vis DRS of SBO, CdS and CdS/SBO nanomaterials. (h) Plots of $(ahv)^2$ versus photo energy (hv) of SBO and CdS.

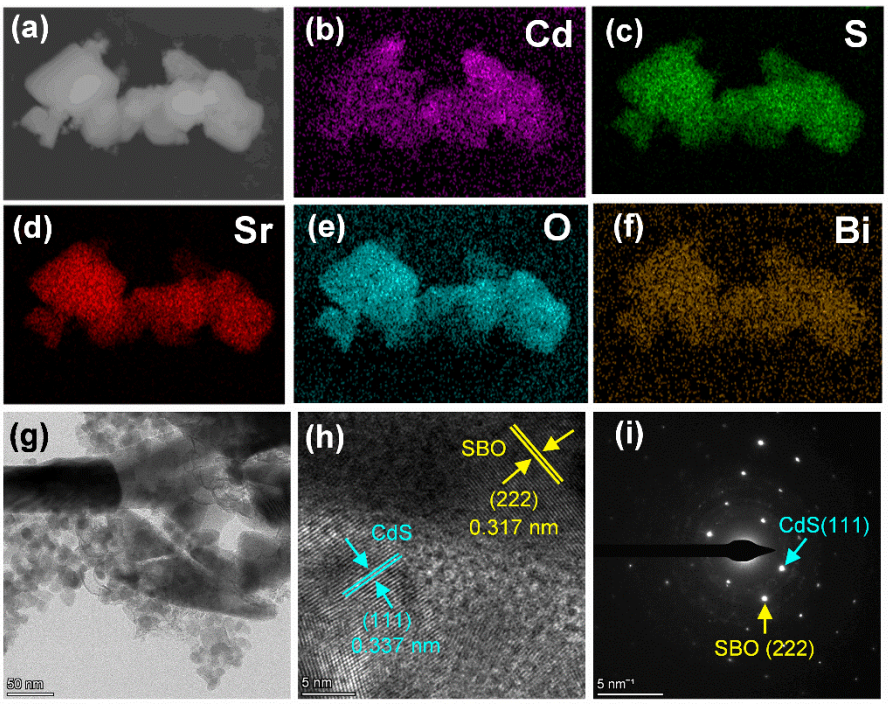

Fig. S5. (a–f) The EDS elemental mappings for the heterostructural CdS/SBO. (g) TEM, (h) HRTEM images and (i) SAED of heterostructural CdS/SBO.

\

Before carrying out systematic experiments, we optimized the proportion of complex SBO, Fig. S6 shows the MM (100 ppm) responses of all chemiresistors under different temperature (50 – 250 °C). It can be seen that the response of 0.05% SBO/CdS chemiresistor exhibits the highest response to 100 ppm MM. Therefore, 0.05% SBO was selected to compound with CdS material to form a heterogeneous structure. Therefore, 0.05% SBO/CdS in the manuscript is uniformly abbreviated as CdS/SBO.

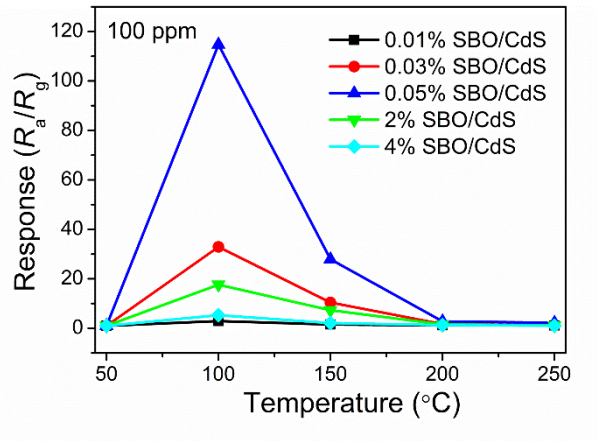

Fig. S6. Responses of all chemiresistors to 100 ppm MM versus the operation temperature.

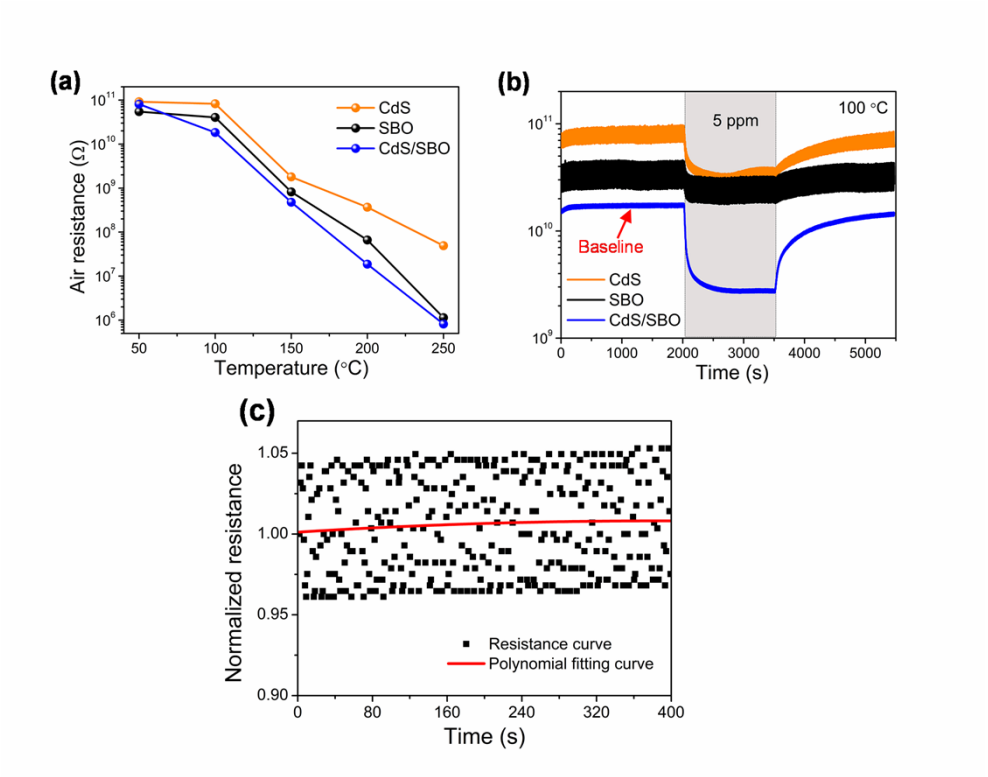

Fig. S7. (a) Air resistance curve with operation temperature of all chemiresistors. (b) Resistance curves of all chemiresistors to 5 ppm MM at 100 °C.(c) Calculation of the noise using the variation in the normalized resistanceof the baseline indicated in Fig. S7b

Table S1 Polynomial fitting data of CdS/SBO chemiresistor to MM gas

Time (s)(s)	yi − y	$(yi - y)^2$
1	-0.00126	1.5876E-06
40	0.01856	0.000344474
80	0.03501	0.0012257
120	-0.01906	0.000363284
160	-0.03765	0.001417523
200	0.03939	0.001551572
240	0.02463	0.000606637
280	0.02063	0.000425597
320	-0.01856	0.000344474
360	-0.0364	0.00132496
400	-0.03287	0.001080437

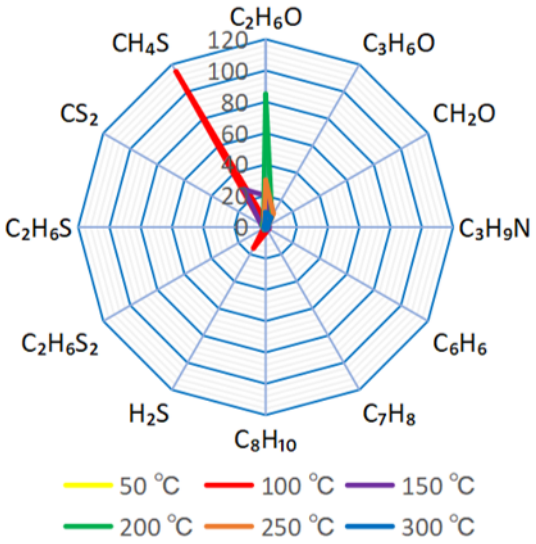

Fig. S8. Radar plot for the response of CdS/SBO chemiresistor toward 12 kinds of vapors (100 ppm), as a function of working temperature ranging from 50 to 300 °C.

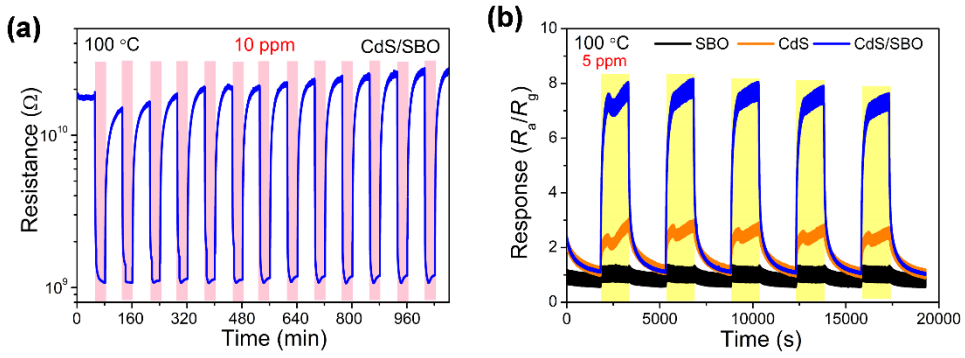

Fig. S9. (a) The resistance repeatability curves of CdS/SBO chemiresistor to 10 ppm MM at 100 °C. (b) The response repeatability curves of three chemiresistors to 5 ppm MM at 100 °C.

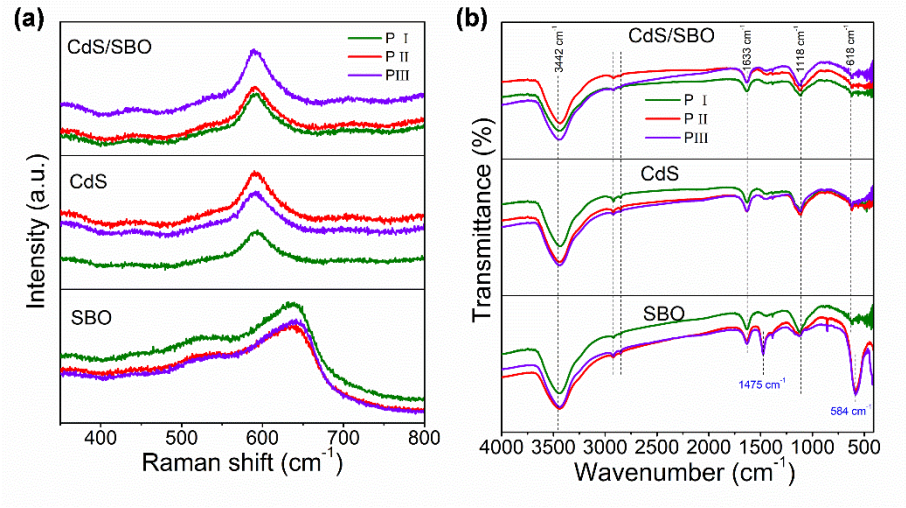

Fig. S10. (a) Raman and (b) FTIR of CdS, SBO and CdS/SBO sensing layer taken on different stages, respectively.

[1] L. Jiang, J. Hu, S. Yan, Y. Xue, S. Tang, L. Zhang, Y. Lv, A novel H_2S cataluminescence sensor based on ZnMn2O4 nanoparticles, Microchemical Journal, 172 (2022) 106990.

[2] K. Zhang, S. Qin, P. Tang, Y. Feng, D. Li, Ultra-sensitive ethanol gas sensors based on nanosheet-assembled hierarchical ZnO-In_2O_3 heterostructures, J Hazard Mater, 391 (2020) 122191.

[3] F. Liu, J. Cao, Z. Yang, W. Xiong, Z. Xu, P. Song, M. Jia, S. Sun, Y. Zhang, X. Zhong, Heterogeneous activation of peroxymonosulfate by cobalt-doped MIL-53(Al) for efficient tetracycline degradation in water: Coexistence of radical and non-radical reactions, J Colloid Interface Sci, 581 (2021) 195-204.

[4] Y. Hao, S. Wang, Q. Sun, L. Shi, A.-H. Lu, Uniformly dispersed Pd nanoparticles on nitrogen-doped carbon nanospheres for aerobic benzyl alcohol oxidation, Chinese Journal of Catalysis, 36 (2015) 612-619.

[5] Y. Cao, X. Huang, Y. Wu, Y.-C. Zou, J. Zhao, G.-D. Li, X. Zou, Three-dimensional ultrathin In_2O_3 nanosheets with morphology-enhanced activity for amine sensing, RSC Advances, 5 (2015) 60541-60548.

[6] Y.V. Kaneti, R.R. Salunkhe, N.L. Wulan Septiani, C. Young, X. Jiang, Y.-B. He, Y.-M. Kang, Y. Sugahara, Y. Yamauchi, General template-free strategy for fabricating mesoporous two-dimensional mixed oxide nanosheetsviaself-deconstruction/reconstruction of monodispersed metal glycerate nanospheres, Journal of Materials Chemistry A, 6 (2018) 5971-5983.